Wind Turbine Interference Mitigation Using a Waveform Diversity Radar

STEVEN I. KRICH, Life Member, IEEE
MONICA MONTANARI
VINCENT AMENDOLARE
PAUL BERESTESKY
Massachusetts Institute of Technology Lincoln Laboratory, Lexington, MA, USA

Interference from the proliferation of wind turbines is becoming a problem for ground-based medium-to-high pulse repetition frequency (PRF) pulsed–Doppler air surveillance radars. This paper demonstrates that randomizing some parameters of the transmit waveform from pulse to pulse, a filter can be designed to suppress both the wind turbine interference and the ground clutter. Furthermore, a single coherent processing interval (CPI) is sufficient to make an unambiguous range measurement. Therefore, multiple CPIs are not needed for range disambiguation, as in the staggered PRFs techniques. First, we consider a waveform with fixed PRF but diverse (random) initial phase applied to each transmit pulse. Second, we consider a waveform with diverse (random) PRF. The theoretical results are validated through simulations and analysis of experimental data. Clutter-plus-interference suppression and range disambiguation in a single CPI may be attractive to the Federal Aviation Administration and coastal radars.

Manuscript received January 28, 2016; revised May 31, 2016 and September 15, 2016; released for publication September 27, 2016. Date of publication February 7, 2017; date of current version April 27, 2017.

DOI. No. 10.1109/TAES.2017.2665143

Refereeing of this contribution was handled by A. Charlish.

Authors' addresses: S. I. Krich, M. Montanari, V. Amendolare and P. Berestesky are with the Massachusetts Institute of Technology Lincoln Laboratory, Lexington, MA 02421, USA, E-mail: (krich.steven@gmail.com; momo@ll.mit.edu; vincent.amendolare@ll.mit.edu; paul.berestesky@ll.mit.edu).

I. INTRODUCTION

Wind power supplies more than 4.5% of the United States electricity portfolio today. Wind is a nationwide affordable natural resource, available on land and offshore; it is renewable, has health and environmental benefits because it reduces air pollution emissions and water consumption, and has also social and economic benefits because it supports the domestic supply chain. It is envisioned that wind power will supply 10% of the national end-use electricity demand by 2020, 20% by 2030, and 35% by 2030 [1]. On the other hand, wind farms bring challenges for air surveillance radars.

The energy produced by wind power is proportional to the swept area and to the wind speed. With these considerations in mind, higher efficiency wind power farms tend to employ larger blade rotors and higher turbine towers. The wind turbine rotating blades create interference, manifested as a broad spectrum of Doppler frequency shifts from both direct path and multipath off the ground. The ground bounce does not change the interference Doppler frequency, but may change its power spectrum. These effects can have a major impact on pulsed–Doppler air/ground surveillance radars, for example, air traffic control (ATC) radars, causing target signal-to-noise ratio (SNR) loss and lower probability of detection, higher false alarm rate, as well as lost tracks. As a result of the proliferation of wind turbines in the USA, there have been many studies on how to mitigate the impact upon nearby radars throughout changes in the radar signal processing [2]–[7]. The techniques proposed in the aforementioned papers involve modifications in the detector stage to discriminate between real targets and wind turbine interference. Further review of these techniques follows in Section I-A.

In this paper, we propose the use of waveform diversity on transmit and coherent processing on receive for a ground-based radar for airborne target surveillance, in order to resolve range ambiguity and suppress the ground clutter, as well as the wind turbine interference.

Traditionally, a pulsed–Doppler radar collects multiple pulses in a coherent processing interval (CPI), using a fixed waveform and pulse repetition frequency (PRF). A medium-to-high PRF is desirable to unambiguously measure the airborne target radial velocity, but range measurements become ambiguous. To resolve the range ambiguity, multiple CPIs are required at different PRFs [8]. A target in a range ambiguity without wind turbine interference is difficult to detect when all range ambiguities fold over into a single interval, as illustrated in Fig. 1.

A random transmit initial phase applied to each pulse, as shown in Fig. 2, enables the design of a filter which suppresses the ground clutter and unambiguously measures the airborne target range using a single CPI [9]. This paper extends the work in [9] to include the suppression of the wind turbine interference, which along with the ground clutter, may be range ambiguous. The range ambiguity can be uniquely determined by processing a single CPI, applying the appropriate Doppler filter to each range ambiguity.

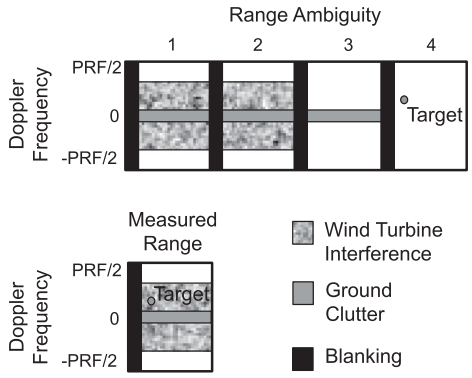

Fig. 1. Range–Doppler space showing four ambiguity regions due to the choice of PRF. The target is in the fourth region. When a conventional radar signal processing is used, the target, the ground clutter, and the wind turbine interference fold over into a single measured range region.

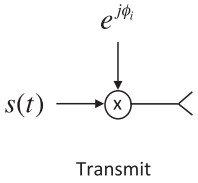

Fig. 2. Random phase radar transmitter. $s(t)$ denotes the transmitted waveform, and φ_i denotes the transmit initial phase for the ith pulse.

Target detection is possible anywhere in the white space in the top picture in Fig. 1. Note that we can also detect very slow (or even zero radial velocity) airborne targets beyond the ground clutter horizon. Two CPIs per dwell may still be needed, due to the receiver blanking during the transmission of the pulses. Additionally, for the same dwell time of a traditional radar, each of these two CPIs can process a larger number of pulses, resulting in improved detection due to increased SNR. In this paper, the algorithm performance is evaluated using the probability of target detection, as in [9], the signal-to-interference-plus-noise ratio (SINR) loss and the Doppler filter pattern.

Unambiguous range measurements and ground clutter suppression can also be performed by randomizing the pulse repetition interval (PRI) [10], [11]. This approach has the advantage of not continually obscuring targets by blanking during transmit and thus uses a single CPI. In this paper, we extend the use of the random PRI to the case when wind turbine interference is present.

This paper is organized as follows. The mathematical derivation of the phase diversity approach and the definitions of the performance metrics are discussed in Section II, and numerical examples for performance evaluation are given in Section II-A. Section II-B compares the phase diversity approach to the constant phase approach utilizing experimental data with wind turbine interference. The PRI diversity approach is addressed in Section III. Finally, Section IV provides the conclusions and possible future investigations.

A. Review of Other Techniques in the Presence of Wind Turbine Interference

Several different approaches have been developed to suppress wind turbine interference for several classes of surveillance radars [2]–[7], which are meant to discriminate between target and wind turbine interference, generally in the detection stage. In [2], the wind turbine interference mitigation is addressed by using several discrimination techniques in predetection, detection and postdetection stages. These techniques include using two channels for elevation discrimination (predetection), an enhanced constant false alarm rate (CFAR) detector and enhanced moving target detector (MTD) algorithm (detection), and improved tracking and classification algorithms (postdetection). In the CFAR detector, the threshold is computed after substituting the returns in the cells showing extremely large power with the average noise power. The enhanced MTD algorithm uses adaptive clutter maps in each individual Doppler filter to suppress the wind turbine interference. The estimation of dynamic clutter maps is also proposed in [3] for ATC radars.

A signal decomposition approach for interference mitigation is proposed in [4], where the radar signal is decomposed into the superposition of an oscillatory component (the moving target has a sparse representation in the Fourier transform domain) and of a transient component (the wind turbine interference has a sparse representation in the short-time Fourier transform domain). The target and interference components are estimated through an L_1-norm minimization problem of a nonlinear cost function, which is solved using an iterative numerical algorithm.

A different approach, proposed for weather radars, attempts to identify the wind turbine interference contaminated cells in the range–Doppler spectrum, or range-azimuth–Doppler spectrum, for the reconstruction of the weather signal, using interpolation [5] or regression [6] techniques. Phased arrays and the minimum variance distortionless response approach are proposed in [7] for interference rejection in Doppler weather radars.

II. STATIONARY GROUND RADAR WITH PHASE DIVERSITY

Consider a stationary ground radar, which is range ambiguous, due to the choice of the PRF. This paper adopts the following notational conventions: nonbold letters to denote scalars, bold lowercase letters to denote vectors, and bold uppercase letters to denote matrices. The superscript H denotes the Hermitian transpose of a vector or matrix. The following notation is used throughout this paper:

1) K_C: number of clutter ambiguity regions;
2) $\mathbf{k}_I$: set of wind turbine interference range ambiguities, not necessarily contiguous;
3) M: number of target range ambiguity regions;
4) N: number of transmitted pulses;
5) $N + M - 1$: number of received PRIs (the radar listens until all the pulses are received for a target in the Mth range ambiguity);

6) φ_i random phase for the ith pulse, $0 \le \varphi_i < 2\pi$. We assume that the initial phases for all pulses are independent and identically distributed, with uniform distribution.

Assuming pulse compression has already been performed, we derive the Doppler filter $\mathbf{w}(f,k)$, where f is the normalized Doppler frequency in the interval $f \in [-0.5, 0.5]$ and $k \in \{1, 2, \ldots, M\}$ is the range ambiguity index. The filter is designed to maintain unit gain on the target and filter the clutter and wind turbine interference from all range ambiguity regions.

Define $\mathbf{v}_0(f) = 1/\sqrt{N} \cdot [1,\ e^{j2\pi f},\ \ldots,\ e^{j2\pi(N-1)f}]^T$ as the canonical steering vector for a pulse–Doppler radar, and $\boldsymbol{\varphi} = [e^{j\varphi_0},\ \ldots,\ e^{j\varphi_{N-1}}]^T$ as the vector of the transmitted initial phases. Then, the steering vector representing the response from a real target or from a wind turbine in the first range ambiguity is

$$\mathbf{v}(f,1) = \left[\mathbf{v}_0^T \odot \boldsymbol{\varphi}^T,\ \mathbf{0}_{M-1}\right]^T \tag{1}$$

where $\mathbf{0}_{M-1}$ denotes a row vectors of $M-1$ zeros and $\odot$ denotes the Hadamard (or element-wise) product. The general steering for the Doppler–range ambiguity pair (f,k) is defined as

$$\mathbf{v}(f,k) = \left[\mathbf{0}_{k-1},\ \mathbf{v}_0^T \odot \boldsymbol{\varphi}^T,\ \mathbf{0}_{M-k}\right]^T. \tag{2}$$

According to (2), the radar has to wait for $k-1$ PRIs before receiving the N pulses from a target situated in the kth ambiguity region. This paper uses all pulses, including the clutter fill pulses, which are usually dropped (see, for example, [9]). The mathematics changes slightly if the clutter fill pulses are dropped.

The output power p_o from filter $\mathbf{w}(f_0,k_0) = \mathbf{v}(f_0,k_0)$ (steered at normalized Doppler frequency f_0 and range ambiguity k_0) to an input signal $\mathbf{v}(f,k)$ is $p_o(f,k) = |\mathbf{v}^H(f_0,k_0)\mathbf{v}(f,k)|^2$. When $k = k_0$, i.e., the filter is designed for the same range ambiguity of the input signal, the output power is

$$p_o = \frac{1}{N^2}\left|\frac{\sin[\pi(f-f_0)N]}{\sin[\pi(f-f_0)]}\right|^2 \tag{3}$$

which peaks with magnitude 1 when $f = f_0$ and is a sinc-shaped function, as the usual Doppler response in a radar with constant phase. For all other range ambiguities, i.e., $k \ne k_0$, after some calculations, we have

$$\left|\mathbf{v}^H(f_0,k_0)\,\mathbf{v}(f,k)\right|^2 = \sum_m \sum_n e^{j(\gamma_m+\gamma_n)} e^{-j2\pi(f-f_0)(m-n)} \tag{4}$$

where γ_i is a random variable uniformly distributed in $[0, 2\pi]$ and the summations run from $m,n = 0$ to $m,n = N-1-|k-k_0|$. When we take the expectation of the output power, the right-hand side term in (4) is not zero only when $n = m$, and thus, we have

$$E\{p_o(f,k)\} = \frac{N-|k-k_0|}{N^2}. \tag{5}$$

Therefore, for large N, steering vectors in different range ambiguities are almost orthogonal even if they are steering to the same Doppler frequency (i.e., $f = f_0$). This is the enabler allowing for discriminating between targets in different range ambiguities and for designing a Doppler filter with different filtering properties in each range ambiguity as described below. Note that this newly designed bank of Doppler filters allows the detection of targets over the clutter horizon even at zero Doppler frequency. On the contrary, in traditional pulse–Doppler radars (where the initial phase of the transmit pulse is constant), the target steering vectors at the same Doppler frequency from different ambiguities would be highly correlated, preventing the discrimination of range ambiguity or the detection of targets at Doppler frequencies competing with the ground clutter or the wind turbine interference.

To design the filter, we model the $(N+M-1)\times(N+M-1)$ interference covariance matrix as

$$\mathbf{R} = \mathbf{R}_C + \mathbf{R}_I + \sigma_n^2\mathbf{I} \tag{6}$$

where $\mathbf{R}_C$ is the ground clutter covariance matrix, $\mathbf{R}_I$ is the wind turbine interference covariance matrix, and $\mathbf{I}$ is the identity matrix representing thermal noise with variance σ_n^2. The ground clutter covariance matrix is modeled as

$$\mathbf{R}_C = \sum_{k=1}^{K_C}\int_{-\delta}^{\delta} p_C(f,k)\mathbf{v}(f,k)\mathbf{v}^H(f,k)df. \tag{7}$$

The integral accounts for ground clutter motion over Doppler frequencies $f \in [-\delta, \delta]$, as, for example, foliage motion due to wind [12], and $p_C(f,k)$ represents the clutter power spectral density (PSD), which can be modeled using parameters as in [12] for a variety of different types of terrain, or measured *in situ* by the radar using a low PRF to avoid range ambiguities. The wind turbine interference covariance matrix is similarly modeled as

$$\mathbf{R}_I = \sum_{k\in\mathbf{k}_I}\int_{-\Delta}^{\Delta} p_I(f,k)\mathbf{v}(f,k)\mathbf{v}^H(f,k)df \tag{8}$$

where the interference PSD $p_I(f,k)$ is defined in $f \in [-\Delta, \Delta]$. The intent of the paper is to develop a methodology of dealing with wind turbine interference and not to delve deeply into the nature of the wind turbine PSD $p_I(f,k)$. This could be measured *in situ* by the radar, or modeled using measured data, as, for example, in [13]–[15]. Since the Doppler filters will be designed upon measuring the interference Doppler spectrum, they will suppress both direct path, multipath, and even a Doppler shift from a bounce off of a moving blade. These models could be adjusted based upon the prevailing winds. To ensure suppression of the ground clutter and the wind turbine interference, it might be preferable to overestimate δ, Δ, $p_C(f,k)$, and $p_I(f,k)$.

The colored-noise matched filter for a target at Doppler frequency f and ambiguity region k is [16], [17]

$$\mathbf{w}(f,k) = \frac{\mathbf{R}^{-1}\mathbf{v}(f,k)}{\mathbf{v}^H(f,k)\mathbf{R}^{-1}\mathbf{v}(f,k)}. \tag{9}$$

In this paper, the principal performance metric is the SINR loss ρ, which is defined as the ratio of the SINR

to the SNR, both quantities computed at the output of the matched filter as

$$\rho \triangleq \frac{\text{SINR}}{\text{SNR}}. \tag{10}$$

Given a filter $\mathbf{w}$ and interference-plus-noise covariance matrix $\mathbf{C}$, the SINR is

$$\text{SINR} = \frac{\sigma_T^2 \left|\mathbf{w}^H(f,k)\mathbf{v}(f,k)\right|^2}{\mathbf{w}^H(f,k)\mathbf{C}\mathbf{w}(f,k)} \tag{11}$$

where σ_T^2 is the target power and $\mathbf{w}(f,k)$ is given by (9) and $\mathbf{C} = \mathbf{R}$. When only thermal noise is present, we have $\mathbf{C} = \sigma_n^2\mathbf{I}$, $\mathbf{w} = \mathbf{v}(f,k)$, and the SNR is

$$\text{SNR} = \sigma_T^2 \mathbf{v}^H(f,k)\mathbf{v}(f,k)/\sigma_n^2. \tag{12}$$

Using (9)–(12), and considering that the clutter and interference PSDs are purposely overestimated, the SINR loss ρ is bounded as follows:

$$\frac{\mathbf{v}^H(f,k)\mathbf{R}^{-1}\mathbf{v}(f,k)}{\mathbf{v}^H(f,k)\mathbf{v}(f,k)}\sigma_n^2 \le \rho \le 1. \tag{13}$$

The lower bound represents the worst SINR loss and the upper bound corresponds to no loss due to the presence of the interference. The specific value of ρ depends on how much the clutter and the interference are overestimated in (7) and (8).

The second performance metric is the Doppler filter pattern, or response, which is the filter output power when the input signal is $\mathbf{v}(f,k)$ in (2) and the filter $\mathbf{w}$ in (9) is matched to a target with normalized Doppler frequency f_T and range ambiguity k_T as

$$P(f,k) = \left|\mathbf{w}^H(f_T,k_T)\mathbf{v}(f,k)\right|^2. \tag{14}$$

Finally, the last performance metric evaluated in this paper is the probability of detection P_D, derived following a generalized likelihood ratio test approach [9], [16]. Denote with

$$\mathbf{y} = \sigma_T\mathbf{v}(f_T,k_T) + \mathbf{c} + \mathbf{i} + \mathbf{n} \tag{15}$$

the pulse compressed signal in the range bin under test, where $\mathbf{c}$ is the clutter vector with covariance matrix $E\{\mathbf{c}\mathbf{c}^H\} = \mathbf{R}_C$, $\mathbf{i}$ is the interference vector with covariance matrix $E\{\mathbf{i}\mathbf{i}^H\} = \mathbf{R}_I$, and $\mathbf{n}$ is the thermal noise vector, with covariance matrix $E\{\mathbf{n}\mathbf{n}^H\} = \sigma_n^2\mathbf{I}$. Interference, clutter, and noise are modeled as independent, complex, normal, zero-mean random processes. With these assumptions, the probability of detection is computed as [16]

$$P_D = Pr\Big\{ \max_{f,k} \left|\mathbf{w}(f,k)^H\mathbf{y}\right|^2 \ge T \cap \arg\max_{k,f} \left|\mathbf{w}(f,k)^H\mathbf{y}\right|^2 = (f_T,k_T)\Big\} \tag{16}$$

where T is the threshold that guarantees the desired false alarm rate P_{FA}, and symbol $\cap$ means that both conditions must be met.

TABLE I
Parameter Values for the Example Scenario

Parameter	Value
N	100
M	3
K_C	2
CNR	30 dB
σ	0.0025
$\mathbf{k}_I$	1
Δ	0.3
INR	30 dB
P_{FA}	10^{-3}
k_T	3
f_T	0, 0.3

A. Performance Analysis

To evaluate the performance of the phase diversity radar, we analyze two cases. In the first case, clutter is added to thermal noise, similarly as in [9], while in the second case, we also include wind turbine interference.

Let us consider the first example, where clutter and noise are the only disturbances. As mentioned above, clutter and thermal noise are modeled as complex Gaussian zero-mean random processes. Assume that the number of pulses is $N = 100$, the number of target range ambiguities is $M = 3$, and that the clutter PSD has a Gaussian shape [18]

$$p_C(f,k) = \frac{\sigma_C^2}{k^4} \cdot \frac{1}{\sqrt{2\pi}\sigma} \exp\left\{-\frac{f^2}{2\sigma^2}\right\} \tag{17}$$

where $\sigma = 0.0025$, and σ_C^2 is derived from the clutter-to-noise ratio (CNR) as

$$\text{CNR} = \frac{\sigma_C^2 \sum_{k=1}^{K_C} k^{-4}}{\sigma_n^2} \tag{18}$$

with $K_C = 2$ and CNR = 30 dB. In this case, the clutter spreads over the 6% of the total Doppler frequency region. Table I summarizes the parameters used in this section to evaluate the radar performance.

Fig. 3 shows the lower bound of the SINR loss ρ in (13), averaged with respect to the random phase sequence. This lower bound represents the worst case, as a function of the target normalized Doppler frequency, for each range ambiguity. Note that a stationary target (or null radial velocity) in the third range ambiguity has minimal loss, since there is no ground clutter in this region. This is a unique property of a coherent phase diversity radar, which is able to resolve range ambiguities and therefore separate a target from the clutter which lies in a different ambiguity. The SINR loss ρ in the third ambiguity for a constant phase pulse–Doppler radar is also shown in the plot and is similar to the loss of the phase diversity radar in the first two ambiguities, where clutter is present. For comparison purposes, the constant phase radar processes all pulses, including the clutter fill pulses. In the third ambiguity and for Doppler frequencies outside the clutter region, the performance of the phase diversity radar is only a fraction of dB lower

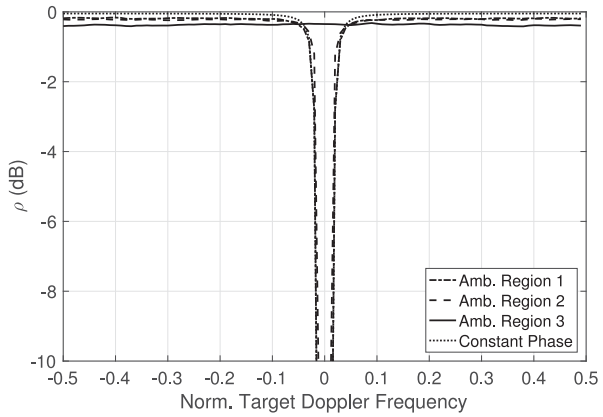

Fig. 3. Worst case for the SINR loss ρ in (13), shown versus normalized target Doppler frequency; $N = 100$, $M = 3$, $K_C = 2$, CNR = 30 dB, 6% clutter Doppler spread. The actual SINR loss lies between the depicted SINR loss and 0 dB (corresponding to no loss). The lines correspond to the limit SINR loss for a phase diversity radar in the three ambiguity regions, respectively. The phase diversity radar can detected a target at zero Doppler frequency in the third ambiguity region. The penalty for doing this a minimal loss at other Doppler frequencies.

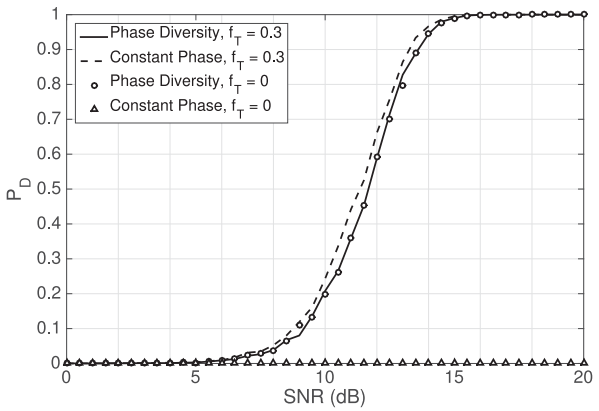

Fig. 4. Probability of detection as a function of target SNR; $N = 100$, $M = 3$, $K_C = 2$, $CNR = 30$ dB, 6% clutter Doppler spread, $f_T = 0.3,\ 0$, $k_T = 3$, $P_{FA} = 10^{-3}$. When $f_T = 0.3$, the minimal loss of the random phase radar with respect to the constant phase radar is the penalty for being able to detect targets at zero Doppler frequency in the third ambiguity region.

than the performance of the constant phase radar. Given the SINR losses for the different range ambiguities, we can compute the corresponding minimum detectable velocities (MDVs) as

$$\text{MDV} = \frac{\lambda}{2} f_{\text{mdv}} \tag{19}$$

where λ is the wavelength and $f_{\text{mdv}} = (f_U - f_L)/2$ represents the minimum detectable Doppler frequency, with f_L and f_U denoting respectively the Doppler frequencies above and below the clutter-plus-interference main lobe at which acceptable SINR loss is achieved [19], i.e., $\rho \geq L$. Assuming PRF = 10 kHz, central transmit frequency $f_c = 2$ GHz, and $L = -12$, which corresponds to acceptable performance equal to 50% of the radar's maximum detection range, the MDV for the constant phase case is constant for all range ambiguities, and equal to 9.7 m/s. In the case of phase diversity, the MDV for $k = 1$ assumes the same value as the MDV in the constant phase case, and decreases to 7.4 m/s for $k = 2$. After the clutter horizon range, corresponding to $k \geq 3$, the MDVs for all range ambiguities are zeros.

The probability of detection for the phase diversity radar is shown in Fig. 4 as a function of the target SNR defined in (12), together with the probability of detection for the constant phase radar. The probability of false alarm has been set equal to $P_{\text{FA}} = 10^{-3}$, and the probability of detection has been computed using 10^5 Monte Carlo simulations. The target range bin belongs to the third ambiguity ($k_T = 3$) and its normalized Doppler frequency is either $f_T = 0.3$ or $f_T = 0$. In the first case, the target Doppler frequency is outside the clutter region to allow for detections from the constant phase radar, which would be otherwise unable to detect the target in clutter. The second example represent the case when only the phase diversity approach enables detection. Outside the clutter region, the phase diversity radar requires a slightly higher SNR with respect to the constant phase radar, in order to achieve the same probability of detection. This result is in agreement with the results shown in Fig. 3, where it was shown that the SINR loss for the phase diversity radar is only a fraction of dB lower than the SINR loss for a constant phase radar. This minimal loss is the penalty to pay to resolve range ambiguity and allow for detection at zero Doppler frequency in ambiguities without clutter, as shown in the plot for the case $f_T = 0$. The probabilities of detection for a random phase and a constant phase radar have also been compared in [9], which shows a larger loss for the random phase radar with respect to the constant phase radar. The discrepancy is partially due to the fact that in [9] the number of clutter ambiguities is larger and the clutter fill pulses are dropped. However, we were unable to replicate the results in [9] using the same parameter values. Finally, we evaluate the Doppler filter pattern in Fig. 5, where the filter is matched to a target with $f_T = 0$ and $k_T = 3$. The pattern is computed separately for each range ambiguity region. Note that this filter has a typical untapered pattern roll-off in the third range ambiguity region. As expected, the ground clutter around zero Doppler frequency is filtered out in the first two ambiguity regions, and the average sidelobe level is -20 dB, according to $1/N$, with $N = 100$. The sidelobes can be lowered in the third region adding another term to the covariance matrix $\mathbf{R}$ in (6), similar to (7) and (8), selecting the appropriate frequency support outside the main lobe. Applying sidelobe control will slightly increase the width of the main lobe, as shown in Fig. 5(a) with the dashed line. The patterns in the first and second region are not shown in the figure because they resemble the patterns without sidelobe control in the corresponding regions.

In the second example, the wind turbine interference is added to clutter and thermal noise in the first range ambiguity ($\mathbf{k}_I = 1$). The interference is modeled as a complex Gaussian zero-mean random process, independent from

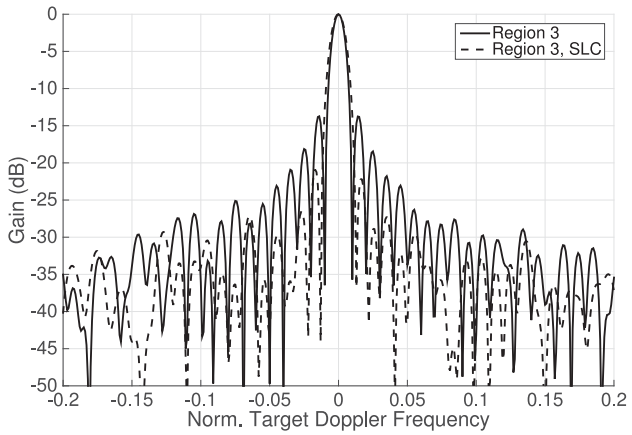

(a)

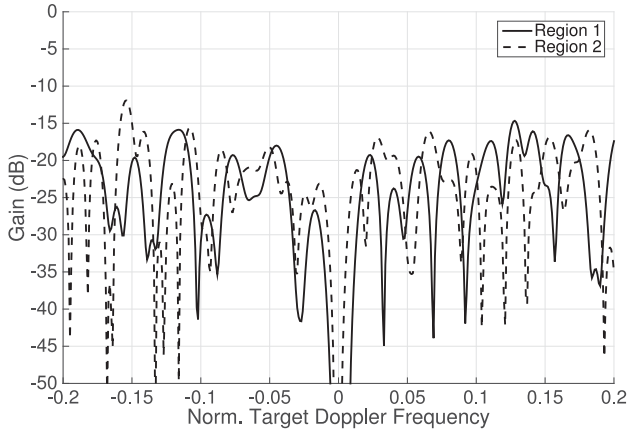

(b)

Fig. 5. Doppler filter pattern for a filter matched to $f_T = 0$ and $k_T = 3$; $N = 100$, $M = 3$, $K_C = 2$, CNR $= 30$ dB, 6% clutter Doppler spread. (a) Pattern for the third ambiguity region, with or without sidelobe control, while (b) shows the response to targets in the first and second ambiguity regions.

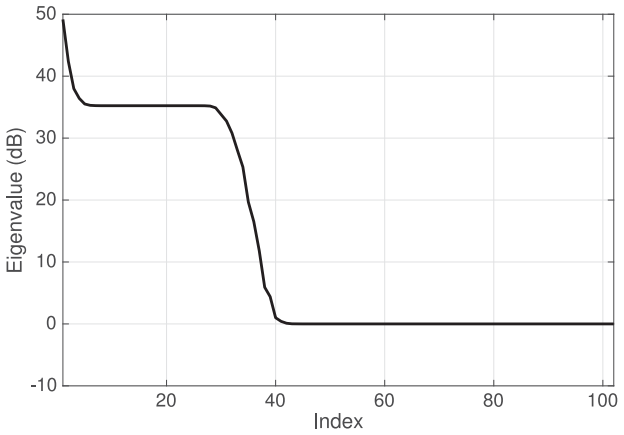

Fig. 6. Eigenspectrum with clutter ($K_C = 2$, CNR $= 30$ dB) and interference ($K_I = 1$, INR $= 30$ dB) in addition to thermal noise (0 dB floor); $N = 100$, $M = 3$, 6% clutter Doppler spread, 30% wind turbine interference Doppler spread.

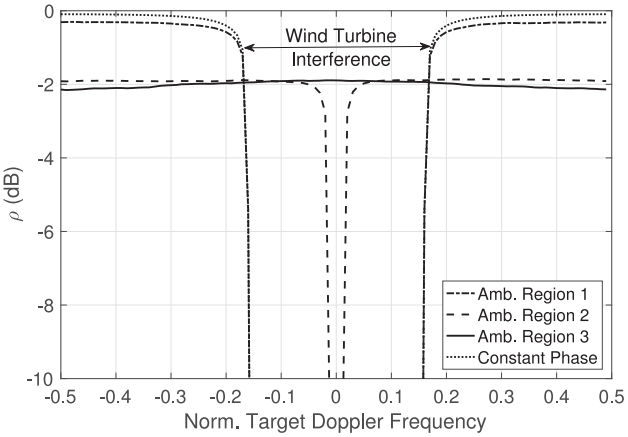

Fig. 7. SINR loss ρ versus normalized target Doppler frequency; $N = 100$, $M = 3$, $K_C = 2$, CNR $= 30$ dB, 6% clutter Doppler spread, $\mathbf{k}_I = 1$, INR $= 30$ dB, 30% wind turbine interference Doppler spread. The penalty for being able to detect zero radial velocity targets is an additional SINR loss for targets outside the clutter and interference Doppler space.

clutter and thermal noise. The interference PSD is constant over its frequency support as

$$p_I(f,k) = \sigma_I^2 \text{rect}\left(\frac{f}{\Delta}\right) \tag{20}$$

where rect$(\frac{f}{\Delta})$ denotes the rectangular function and is equal to 1 when $-\Delta/2 \le f \le \Delta/2$, and is 0, otherwise. The model used in (20) is not realistic for a real wind turbine, but it is useful to understand and illustrate the mathematics and the results. Note that all Doppler frequencies are normalized to the PRF and no attempt is made to discuss actual velocities. When applied to real wind turbine mitigation, the designer needs to delve deeply into an appropriate model for $p_I(f,k)$. The variance σ_I^2 is derived from the interference-to-noise ratio (INR) as

$$\text{INR} = \frac{\sigma_I^2 \Delta \sum_{k \in \mathbf{k}_I} k^{-4}}{\sigma_n^2} \tag{21}$$

where $\Delta = 0.3$ and INR $= 30$ dB. The interference subspace spans 30% of the entire Doppler frequency space. This is shown in Fig. 6, which depicts the eigenspectrum of the covariance matrix in (6), with the choice of parameter values in Table I. The dominant eigenvalues correspond to the clutter subspace, the first flat region corresponds to the more extended interference subspace due to the wind turbines, and 0 dB represents the thermal noise space, which covers the entire Doppler space.

Fig. 7 shows the SINR loss ρ in the three ambiguity regions for the phase diversity radar, as well as the SINR loss in the third region for the constant phase radar. The performance of the constant phase radar is similar in all ambiguity regions, therefore it is shown only in the third region for clarity. The loss of about -2 dB for the phase diversity radar in the second and third regions is caused by the fact that a signal in these ambiguities has a larger component into the disturbance subspace, with respect to a signal in the first ambiguity. In fact, if we build the disturbance subspace using the eigenvectors whose eigenvalues are 10 dB higher than the noise power, and we compute the power

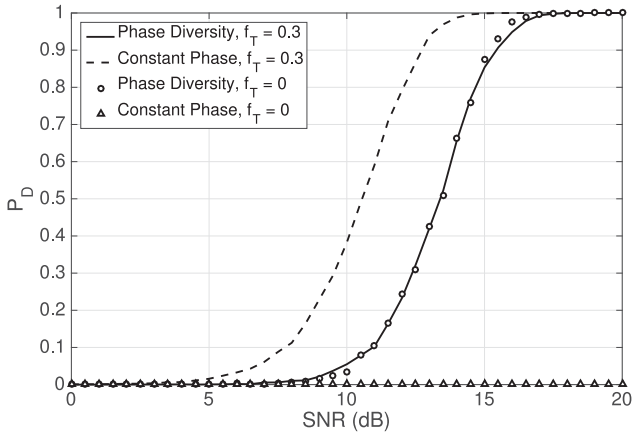

Fig. 8. Probability of detection as a function of target SNR; $N = 100$, $M = 3$, $K_C = 2$, CNR $= 30$ dB, 6% clutter Doppler spread, $\mathbf{k}_I = 1$, INR $= 30$ dB, 30% wind turbine interference Doppler spread, $f_T = 0.3,\ 0$, $k_T = 3$, $P_{FA} = 10^{-3}$. The penalty for being able to detect zero radial velocity targets is an SINR loss for targets outside the clutter and interference Doppler space, resulting in a detection loss.

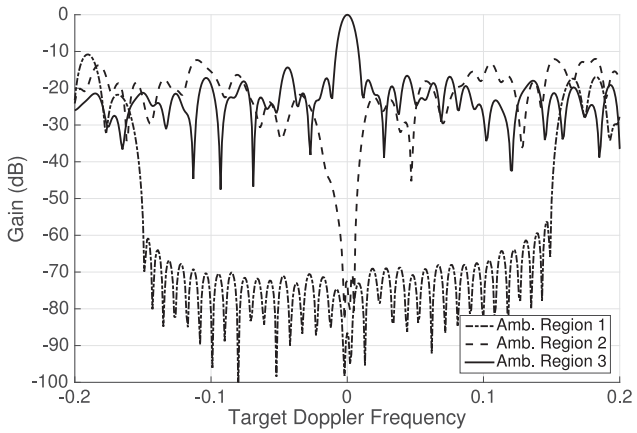

Fig. 9. Doppler filter pattern for a filter matched to $f_T = 0$ and $k_T = 3$; $N = 100$, $M = 3$, $K_C = 2$, CNR $= 30$ dB, 6% clutter Doppler spread, $\mathbf{k}_I = 1$, INR $= 30$ dB, 30% wind turbine interference Doppler spread.

of the signal projected onto the interference disturbance as $a_k = \|\mathbf{U}\mathbf{U}^H\mathbf{v}(f,k)\|^2$, where $\mathbf{U}$ is the matrix assembling the disturbance eigenvectors, the projection onto the disturbance subspace has a higher power when $k = 2, 3$, with respect to $k = 1$. Using 10^3 Monte Carlo realizations of the phases φ_i, and selecting $f = 0.3$, the average powers are $a_1 = 0.017$, $a_2 = 0.307$, and $a_3 = 0.312$.

In this case, using PRF $= 10$ kHz and $f_c = 2$ GHz, we have MDV $= 112.5$ m/s in all range ambiguities for the constant phase case, while for the phase diversity case, the MDV starts at about the same level in the first range ambiguity and decreases to 7.4 m/s in the second range ambiguity, as in the previous example. Once again, MDV $= 0$, when $k \geq 3$.

The penalty for being able to detect low-velocity targets is a probability of detection loss with respect to the constant phase radar for targets outside the clutter Doppler spread. In this example, the -2 dB SINR loss in the second and third ambiguities is in agreement with the result shown in Fig. 8, where the probability of detection is plotted as a function of the target SNR when $f_T = 0.3,\ 0$, $k_T = 3$, and $P_{FA} = 10^{-3}$. With interference, we need approximately 2 dB additional target SNR to obtain the same probability of detection of a constant phase radar, for a target outside the clutter Doppler spread.

Fig. 9 shows the Doppler pattern for the three ambiguity regions, when the filter is matched to a target with $f_T = 0$ and $k_T = 3$. For clarity, only the Doppler frequencies that satisfy $-0.2 \leq f \leq 0.2$ are shown in the plot. Note that the sidelobes are higher with respect to the ones in Fig. 5, where only clutter was added to thermal noise. The reason for the higher sidelobes is that now more degrees of freedom have been used to null the disturbance.

If we want to improve the SINR loss in Fig. 7, we can double the PRF and keep the same CPI duration. Under this assumption, the number of pulses is doubled $N = 200$, the normalized Doppler frequency support for the clutter and

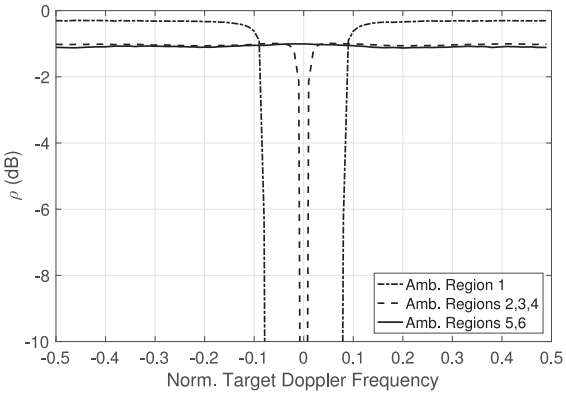

Fig. 10. SINR loss ρ versus normalized target Doppler frequency. The PRF is doubled and the CPI duration is the same as before, resulting in doubling the number of pulses; $N = 200$, $M = 6$, $K_C = 4$, CNR $= 30$ dB, 3% clutter Doppler spread, $\mathbf{k}_I = 1$, INR $= 30$ dB, 15% wind turbine interference Doppler spread. The loss in the interference-free regions has improved by 1 dB with respect to Fig. 7.

interference is halved, and the number of range ambiguities is doubled, $M = 6$. To keep the average power constant, the pulse length can be halved. It is assumed that the ground clutter spans the same range extent and, thus, it occupies now the first four ambiguities $K_C = 4$, and that the wind turbines are located in a narrow range window and thus are located only in the first ambiguity, $\mathbf{k}_I = 1$. Fig. 10 shows the SINR loss ρ for this example. The SINR loss ρ for all regions but the first has improved from -2 to -1 dB. In conclusion, increasing the PRF in the presence of wind turbine interference may prove beneficial, even if there is no interest in detecting targets at higher Doppler frequencies.

B. Results From Experimental Data

The theoretical results have been validated from experimental data collected at the Millstone Hill Observatory, in Westford, MA, USA, using both phase diversity and conventional constant phase. There was one illuminated wind turbine, ground clutter, and targets of opportunity in a different range ambiguity than the wind turbine. The radar

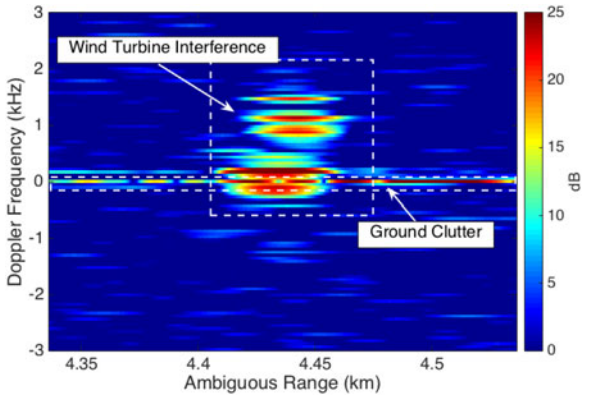

Fig. 11. Range–Doppler map using a constant phase waveform. Ground clutter and wind turbine interference are overlapped in the unambiguous region. Possible targets of interests are masked by the range-ambiguous return from the wind turbine.

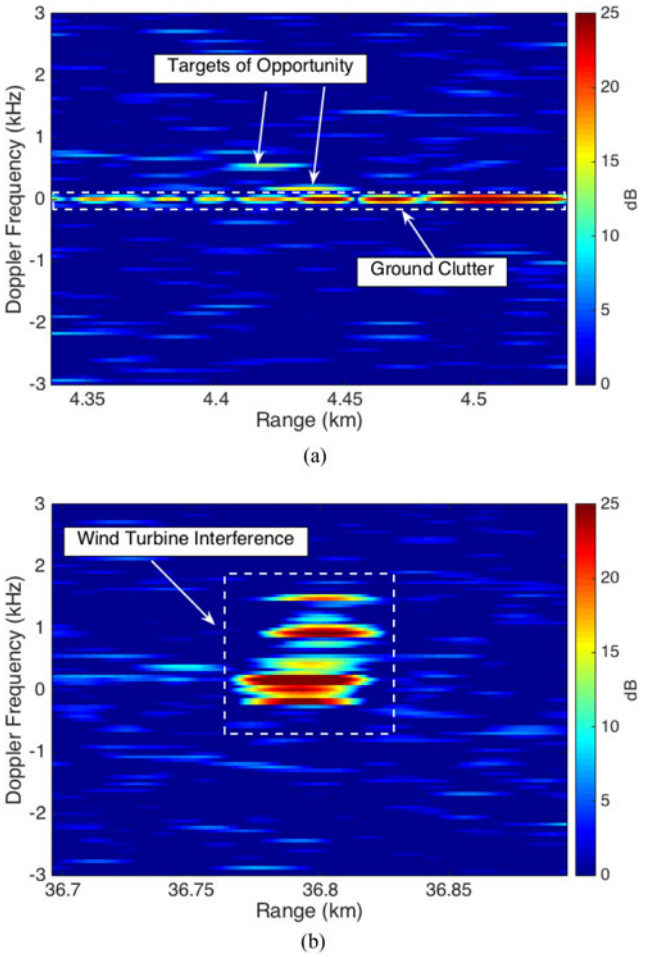

Fig. 12. (a) Range–Doppler maps using phase diversity for the first range ambiguity, where ground clutter and two targets of interest are present, and for the (b) seventh range ambiguity, where only wind turbine interference is present. Range measurement has been disambiguated.

was operating at a frequency of $f_c = 9.7$ GHz, PRF = 28 kHz, and $N = 512$ pulses in a CPI. The phase diversity Doppler filters were designed with $K_C = 1$, $\mathbf{k}_I = 7$, $\delta = 162$ Hz, $\Delta = 1.55$ kHz, CNR = 60 dB, and INR = 40 dB. The Doppler filter responses are similar to those depicted in Section II-A, with sidelobes around -27 dB, due to $N = 512$. The turbine has three blades, with rotor diameter equal to 82 m. The maximum rotational speed is 14.4 r/min, corresponding to a maximum blade tip speed equal to 61.8 m/s and maximum Doppler frequency equal to 4 kHz. The observed maximum Doppler frequency is lower than 4 kHz, due to either slower rotating blades, or the orientation of the rotation plane with respect to the radar, or the position of the blades during the radar measurement, or a combination of the previous reasons. For faster rotating blades, a higher Doppler frequency will be observed, and the Doppler filters will be designed accordingly, with a larger Δ in (8).

Figs. 11 and 12 show the range–Doppler image without and with phase diversity, respectively, where the dB scale is normalized to thermal noise and only the ranges near the wind turbine are shown. The wind turbine is actually in the seventh ambiguity at 36.8 km, but it folds over into the first ambiguity at a range of 4.45 km in Fig. 11, thereby obscuring any nearby targets. The ground clutter is clearly visible at zero Doppler frequency. Fig. 12 shows the results with phase diversity for ranges near 4.45 km and 36.8 km, respectively. In Fig. 12(a), the wind turbine interference is no longer obscuring the two targets of opportunity at Doppler frequencies $f_{T1} = 150$ Hz and $f_{T2} = 550$ Hz. Note that the wind turbine image in Fig. 11 is very similar to the image in the seventh range ambiguity in Fig. 12(b). Moreover, the image in Fig. 12(b) corresponds to a range ambiguity beyond the clutter horizon, therefore no ground clutter is present.

III. GROUND STATIONARY RADAR WITH PRI DIVERSITY

The phase diversity approach in Sections II and II-A can be generalized to arbitrarily diverse transmit waveforms with irregular pulse modulation and variable PRI. A general framework that uses arbitrary waveforms for clutter suppression was presented in [10]. The applicability of such diverse waveforms is extended here to suppress also wind turbine interference.

Arbitrary waveforms have many advantages, such as target detection that is both range and Doppler frequency unambiguous and free of range–Doppler frequency blind zones, therefore enabling surveillance in a single CPI. Processing these waveforms has a higher computational complexity with respect to the traditional pulse–Doppler processing and the phase diversity processing discussed above. Future work may include investigations for developing suboptimal techniques that will improve the computational efficiency.

Here, the standard notation utilized in Sections II and II-A is generalized to arbitrary transmit waveforms, whereas previously we considered transmissions consisting of N regularly spaced pulses, we will now treat waveforms consisting of N regularly spaced samples. Consider

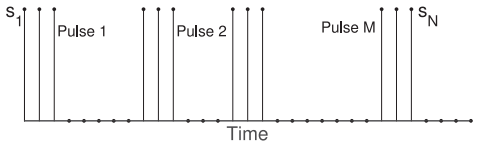

Fig. 13. Modulus of transmitted waveform samples in a CPI, with constant pulse width and variable PRI.

a transmit waveform vector

$$\mathbf{s} = [s_1 \quad s_2 \quad \cdots \quad s_N]^T. \tag{22}$$

A notional waveform is depicted in Fig. 13. For this multiple pulse waveform, the gaps in transmission time are represented by zero values in the transmitted waveform vector. The arbitrary definition allows for nonuniform pulse spacing, as shown in this example. When the radar cannot simultaneously transmit and receive, many samples in the received signal vector will have zero value (blanking) during transmission. To take into account the missing received data, define r_i, with $i = 1, \ldots, N + M - 1$, as

$$r_i = \begin{cases} 1, & \text{transmitter is ON} \\ 0, & \text{transmitter is OFF.} \end{cases} \tag{23}$$

Some portion of relevant received signal will be missing while the receiver is OFF, which will result in an eclipsing loss. Similar losses can occur for traditional pulse–Doppler waveforms.

The steering vector $\mathbf{v}(f, k)$ for a particular Doppler frequency ambiguity region pair (f, k) is constructed similarly to (2) as

$$\mathbf{v}(f,k) = \frac{1}{\sqrt{N}} \times \left[\mathbf{0}_{k-1},\ s_1 e^{2\pi f},\ \ldots,\ s_N e^{2\pi f N},\ \mathbf{0}_{M-k}\right]^T \odot \mathbf{r} \tag{24}$$

where $\odot$ represents the Hadamard product (element-wise product). In this context, every processed range bin, corresponding to a single sample, behaves as a different range ambiguity in Section II. The covariance matrices for ground clutter and wind turbine interference are computed using (7) and (8), while the matched filter is computed as in (9), using (24) as a steering vector. Matrix and vector sizes are now on the order of the number of waveform samples, instead of the number of pulses in Section II.

In the following simulation, consider $M = 100$ transmit pulses, which are linearly frequency modulated (LFM), with bandwidth BW = 1 MHz and pulse width PW = 2 μs. The CPI is divided into adjacent windows of 20 μs each, and the initial sample for each pulse is randomly positioned in the corresponding time window.[1] The number of samples is $N = 2340$. The filter $\mathbf{w}$ is steered to a target with $f_T = 0$ Hz and $k_T = 40$ km. The clutter and interference spectral densities are modeled similarly to (17) and (20).

[1]The position index is uniformly distributed inside the time window.

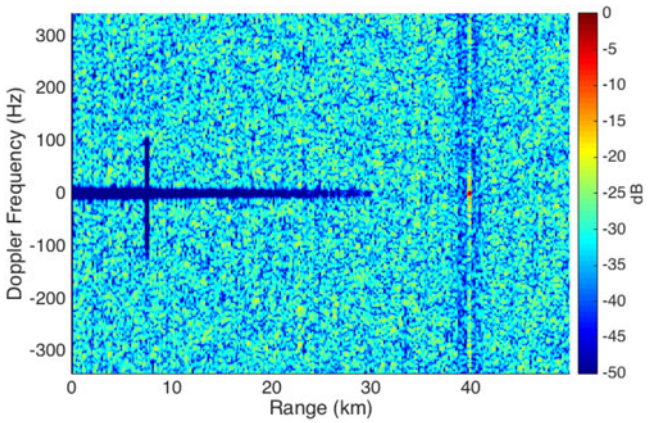

Fig. 14. Doppler filter pattern using an LFM waveform with non–uniform PRI; $M = 100$, $N = 340$, $PW = 2\,\mu$s, $BW = 1$ MHz, $f_T = 0$ and $k_T = 40$ km. The filter pattern has a peak at the steering direction (f_T, k_T) and deep nulls at the ground clutter and wind turbine interference positions.

The CNR is modeled as

$$\text{CNR} = \begin{cases} 10^4, & 0 \le k \le k_1 \\ \dfrac{10^4 k_1^4}{k_2^4 - k_1^4}\left[\left(\dfrac{k_2}{k}\right)^4 - 1\right], & k_1 \le k \le k_2 \\ 0, & k > k_2 \end{cases} \tag{25}$$

where $k_1 = 5$ km and $k_2 = 30$ km. A single wind turbine interference is situated at $\mathbf{k}_I = 7.5$ km. Fig. 14 shows the filter response (14) at the range/Doppler values of interest. The maximum of the sidelobe levels measured approximately -20 dB, according to $1/M$, with $M = 100$. There are no ambiguity peaks in either range or Doppler frequency. Deep nulls are visible in the regions where the ground clutter and the wind turbine interference have been defined. For this particular case, the SINR loss relative to a case with an ideal matched filter and no eclipsing loss is -4.1 dB.

IV. SUMMARY

Waveform diversity on transmit enables a medium-to-high PRF ground–based radar to measure target range unambiguously with a single CPI and filter out the ground clutter and wind turbine interference. This may be beneficial to avoid disambiguation errors for radars operating with a large target population. Depending upon the lay downs of wind turbines, the added benefit is the ability to coexist with nearby wind farms. Furthermore, there is no need to change the random phase sequence from CPI to CPI. Although not studied here, any sequence of phases with low autocorrelation sidelobes, such as random biphase modulation [20], is equivalently effective. The performance of a phase diversity radar has been thoroughly evaluated and compared with the performance of a constant phase radar in the presence of wind turbine interference. Additionally, a waveform diversity example with random PRIs has been shown to provide range disambiguation as well. The theoretical and simulation results have been validated analyzing experimental data.

Future work may include the derivation of random phase sequences with better sidelobe properties over some range–Doppler regions and possible computational complexity reduction. A further enhancement could be to apply knowledge-aided radar techniques, and include, for example, known properties of the turbine, wind speed, and environment [21], [22]. Additionally, also the phase sequence could be derived as the output of a dynamic/instantaneous knowledge-aided optimization technique.

REFERENCES

[1] Wind vision:
A new era for wind power in the United States
U.S. Dept. Energy, Washington, DC, USA, Tech. Rep. DOE/GO-102015-4557 7031, Mar. 2015.

[2] L. Sergey, O. Hubbard, Z. Ding, H. Ghadaki, J. Wang, and T. Ponsford
Advanced mitigating techniques to remove the effects of wind turbines and wind farms on primary surveillance radars
In *Proc. IEEE Radar Conf.*, 2008, pp. 1–6.

[3] R. W. Q. Jia and X. Wang
Recognition and suppression of wind farm clutter via dynamic clutter map
In *Proc. IEEE 11th Int. Conf. Signal Process.*, Oct. 21–25, 2012, vol. 3, pp. 1949–1952.

[4] F. Uysal, U. Pillai, I. Selesnick, and B. Himed
Signal decomposition for wind turbine clutter mitigation
In *Proc. IEEE Radar Conf.*, May 19–23, 2014, pp. 60–63.

[5] B. Perfetti, J. Zheng, and M. Kaveh
Signal processing for wind turbine interference mitigation in doppler weather radars: Data synthesis, clutter detector performance, and spectral interpolation in range-azimuth-doppler
In *Proc. IET Int. Conf. Radar Syst.*, Oct. 22–25, 2012, pp. 1–6.

[6] S. T. F. Nai and R. Palmer
On the mitigation of wind turbine clutter for weather radars using range-doppler spectral processing
IET Radar, Sonar Navig., Feb. 2013, pp. 178–190.

[7] K. L. R.D. Palmer and B. Isom
Wind turbine clutter mitigation using fully adaptive arrays
In *Proc. Eur. Radar Conf.*, Oct. 30–31, 2008, pp. 356–359.

[8] M. I. Skolnik
Introduction to Radar Systems. New York, NY, USA: Mc-Graw-Hill, 2008.

[9] F. ling Lin and M. Steiner
New techniques for radar coherent range ambiguity resolution
In *Proc. IEEE Radar Conf.*, Atlanta, GA, USA, May 1–3 2001, pp. 99–104.

[10] D. Scholnik
Range-ambiguous clutter suppression with pulse-diverse waveforms
In *Proc. IEEE Radar Conf.*, Kansas City, MO, USA, May 23–27 2011, pp. 336–341.

[11] L. Vergara-Dominguez
Analysis of the digital MTI filter with random PRI
IEE Proc., Radar Signal Process., vol. 140, no. 2, pp. 129–137, Apr. 1993.

[12] J. Barrie Billingsley
Low-Angle Radar Land Clutter: Measurements and Empirical Models. Raleigh, NC, USA: SciTech, 2002.

[13] H. J. de Wind, K. H. Kloke, U. Böniger, and H. Pratisto
Comparison of the recorded RCS and spectra of three different wind turbines on l- and s-band
In *Proc. 2015 IEEE Radar Conf.*, Oct. 2015, pp. 266–271.

[14] K. V. Mishra and V. Chandrasekar
Signal analysis and modeling of wind turbine clutter in weather radars
In *Proc. 2010 IEEE Int. Geosci. Remote Sens. Symp.*, Jul. 2010, pp. 3561–3564.

[15] B. Gallardo-Hernando, F. Perez-Martinez, and F. Aguado-Encabo
Statistical characterization of wind turbine clutter in c-band radars
In *Proc. 2008 Int. Conf. Radar*, Sep. 2008, pp. 360–364.

[16] L. Brennan and L. Reed
Theory of adaptive radar
IEEE Trans. Aerosp. Electron. Syst., vol. 9, no. 2, pp. 237–252, Mar. 1973.

[17] C. W. Therrien
Discrete Random Signals and Statistical Signal Processing. New York, NY, USA: Prentice-Hall, 1992.

[18] D. Curtis Schleher
MTI and Pulsed Doppler Radar. Norwood, MA, USA: Artech House, 1991.

[19] J. Ward
Space–time adaptive processing for airborne radars
MIT Lincoln Lab., Lexington, MA, USA, Tech. Rep. 1015, Dec. 1994.

[20] S. R. J. Axelsson
Noise radar using random phase and frequency modulation
IEEE Trans. Geosci. Remote Sens., vol. 42, no. 11, pp. 2370–2384, Nov. 2004.

[21] A. Aubry, A. D. Maio, and M. Naghsh
Optimizing radar waveform and doppler filter bank via generalized fractional programming
IEEE J. Sel. Topics Signal Process., vol. 9, no. 8, pp. 1387–1399, Dec. 2015.

[22] A. Aubry, A. D. Maio, A. Farina, and M. Wicks
Knowledge–aided (potentially cognitive) transmit signal and receive filter design in signal–dependent clutter
IEEE Trans. Aerosp. Electron. Syst., vol. 49, no. 1, pp. 93-117, Jan. 2013.

Steven I. Krich (M'71–LM'09) received the B.S., M.S., and Ph.D. degrees in electrical engineering (information theory) from Cornell University, Ithaca, NY, USA, in 1966, 1968, and 1972, respectively.

Since 1972, he has been a Researcher at MIT Lincoln Laboratory, Lexington, MA, USA, investigating signal processing for radar and communication systems. His current research interests include adaptive signal processing for interference suppression with phased array antennas.

Monica Montanari received the Laurea degree (*cum laude*) and the Ph.D. degree in telecommunication engineering from the University of Pisa, Pisa, Italy, in 1998 and 2002, respectively.

In 2000, she was a Research Assistant at the former NATO SACLANT Undersea Research Center, La Spezia, Italy. In 2002, she joined the former Department of Ocean Engineering at the Massachusetts Institute of Technology, Cambridge, MA, USA, as a Postdoctoral Associate. She is currently a Scientist at MIT Lincoln Laboratory, Lexington, MA. Her general research interests include the area of statistical signal processing, detection and estimation theory, adaptive array processing, with application to airborne and ground radar systems.

Vincent Amendolare received the Ph.D. degree from Worcester Polytechnic Institute, Worcester, MA, USA, in 2010, after conducting research on RF-based indoor geolocation for first responders. His dissertation involved the improvement of a prototype location system by using a novel wireless synchronization approach to obtain time-of-arrival information in strong multipath environments.

After graduating, he joined MIT Lincoln Laboratory, Lexington, MA, and has since worked in the Advanced Concepts and Technologies Group. His focus has been on systems analysis and signal processing applied to developing ground-based radar systems for air and missile defense.

Paul Berestesky received the B.S. degree in computer and systems engineering from Rensselaer Polytechnic Institute, Troy, NY, USA, in 2002, the M.S. degree in general engineering from the University of Illinois, Urbana-Champaign, IL, USA, in 2005, and the M.S. degree in electrical engineering from Northeastern University, Boston, MA, USA, in 2013.

From 2005 to 2007, he was a Control and Handling Qualities Engineer with Sikorsky Aircraft, Stratford, CT, USA. From 2007 to 2013, he was a Radar Systems Engineer with Raytheon, Tewksbury, and Sudbury, MA, USA. After a yearlong stint as a Radar Systems Engineer at Riverside Research, Lexington, MA, he joined MIT Lincoln Laboratory, Lexington, in 2014, where he is currently an associate staff member. His past research includes topics in control systems, radar signal processing, target tracking, and electromagnetics.